Opportunistic localization using LEO signals

Uday Kumar Singh
SnT, University of Luxembourg
Luxembourg, Luxembourg
uday.singh@uni.lu

M. R. Bhavani Shankar
SnT, University of Luxembourg
Luxembourg, Luxembourg
bhavani.shankar@uni.lu

B. Ottersten
SnT, University of Luxembourg
Luxembourg, Luxembourg
Bjorn.Ottersten@uni.lu

***Abstract*—Accurate positioning, navigation, and timing (PNT) are taking a centre stage due to enhanced requirements in safety-critical systems, the emergence of autonomous systems as well as the use of sensor networks in disaster management. While the Global Navigation Satellite System (GNSS) has been a prime source for enabling PNT, the aforementioned use cases would need a complementary solution in case GNSS signals are unavailable, unreliable, or unusable. This work, builds on the existing literature, and considers the use of signals from low Earth orbit (LEO) satellites due to the higher spatial and temporal resolution offered by the evolving and emerging mega-constellations. It builds on the existing LEO PNT works and considers the feasibility of LEO PNT from a system perspective and parameter estimation aspects. It then presents the tracking algorithm fusing information from multiple satellites while incorporating errors in their locations into the state model. Performance evaluation for representative scenarios is undertaken.**

***Keywords*—GNSS denied environments, LEO, PNT, opportunistic localization, EKF, DVB-S2x**

I. Introduction

With an increase in their autonomous functionalities, the requirements for robust and accurate positioning, navigation, and timing (PNT) in safety-critical systems have increased many-fold. Such systems could range from aviation to ground-based IoT sensor networks. Accuracy is needed due to the high spatial resolutions in which such systems operate. Naturally, in the emerging autonomous settings without manual supervision, robustness in localization is needed to counteract intentional and/ or unintentional perturbations to operations, e.g., interference from frequency reuse causing errors in localization [1].

Satellite-based navigation, uses satellites to provide geospatial positioning using Line-of-Sight (LoS) signals; these are processed by user terminals to determine their location - longitude, latitude, and altitude. Such systems are fairly accurate, e.g., GPS signal offers a daily global average user range error $\leq$ 2 m, with 95% probability. In this context, such satellites also transmit timing information used to provide about 10 ns accuracy. Global Navigation Satellite System (GNSS) generically refers to satellite-based navigation offering a global coverage [2]. Currently, many countries offer satellite navigation solutions e.g., GPS (USA), GLONASS (Russia), Galileo (EU), IRNSS (India), and Beidou (China). Satellite-based navigation has been the backbone for localizing terrestrial and non-terrestrial systems for a while.

However, satellite-based navigation has its shortcomings. GNSS signals tend to be weak or unreliable in scenarios like urban canyons or near dense foliage, corrupted due to unintentional interference or intentional jamming or spoofed. In the absence of GNSS, other navigation aids or signals need to be used. In this context, inertial measurement units (IMUs) are used in applications like automotive; these unaided devices offer high accuracy in the short term, but the errors accumulate and eventually diverge, hindering the operations exploiting their data. On the other hand, additional signals of opportunity could be used in GNSS-challenged environments Classical signals include AM/ FM radio, cellular, digital television, and low Earth orbit (LEO) satellites [1], [3]. The literature considers LEO satellites attractive in GNSS-denied environments for the following reasons [1], [3], [4]:

1) LEO satellites are around 20 times closer to Earth compared to GNSS satellites that reside in medium Earth orbit (MEO), thereby resulting in received signals with a higher power.
2) LEO satellites orbit the Earth at much faster rates than GNSS satellites, making their Doppler measurements attractive to exploit.
3) The recent announcements by OneWeb, Boeing, SpaceX (Starlink), Samsung, Kepler, Telesat, and LeoSat to provide broadband internet to the world via satellites will collectively bring thousands of new LEO satellites into operation, making their signals abundant and diverse in frequency and direction.

Literature indicates the following LEO PNT approaches:

1) LEO GNSS : Herein, the LEOs are equipped with navigation payloads and provide PNT services similar to traditional GNSS. While the performance is GNSS-like, it entails additional mission costs.
2) GNSS augmentation with LEO : It considers non-GNSS services offering time and position information from LEO to augment the capabilities of GNSS. The Iridium STL is a case in point that transmits dedicated broadcasts about time and location. Due to their efficient transmission, such broadcasts are able to penetrate into difficult attenuation environments and complement GNSS.
3) Opportunistic navigation with LEO signals : Exploit the communication signals to derive parameters enabling localization. The aim of this overview paper is to investigate opportunistic localization further.

This overview paper presents the scenario and the various models considered in opportunistic PNT with LEO. It subsequently selects the model based on a signal-processing perspective and presents the well-known Extended Kalman Filter (EKF) framework for the position estimate. The system aspects of enabling such estimation are highlighted and representative results are presented.

This work was partially supported by the Luxembourg National Research Fund (FNR) CORE SPRINGER, ref C18/IS/12734677.

II. Scenario and PNT Models

A. Scenario

In this paper, we consider the localization of a User Terminal (UT) with the capability to receive, demodulate and decode LEO signals. The Cartesian coordinates of the UT at time instance t are collected in the vector $\mathbf{r}_r(t)$. The LEO UT under consideration is assumed to be in the coverage of $L \geq 1$ LEO satellites. For this work, it is assumed that the transmissions from the L LEO satellites are received without interference at the UT; these could be scheduled at different frequencies or could be separated spatially using beamforming; either way, the UT is assumed to have multiple receive chains for processing each satellite.

In the following, three existing models for the UT positioning, localization, and tracking are elaborated.

B. PNT Models using LEO

Three models are used in the context of LEO PNT; these largely follow the models used in classical GNSS and are presented below in detail.

1) Pseudorange Measurements: Let $\mathbf{r}_s^l(t)$ be the Cartesian coordinate of the lth LEO satellite at time instance t in the same reference system as the UT. The true time-of-flight solves the equation, $\tau_l(t) = \frac{\|\mathbf{r}_r(t) - \mathbf{r}_s^l(t-\tau_l(t))\|^2}{c}$, where c is the speed of light and $\|\cdot\|$ is the l_2 norm. However, additional perturbations contaminate the readings resulting in the use of the word *pseudorange*. The perturbations include,

- Clock biases of LEO receiver and the l^{th} LEO satellite transmitter respectively at time instance t denoted by $\delta t_r(t)$ and $\delta t_s^l(t)$ respectively.
- The delays introduced by the propagation through ionosphere and troposphere for transmissions from the lth satellite at time t given by, $\delta t_T^l(t)$ and $\delta t_I^l(t)$.

Accordingly, the LEO receiver extracts pseudorange measurements from the lth satellite, $l \in [1, L]$, denoted by, ρ_l, using the corresponding time-of-flight. The time-of-flight can be obtained, as in GNSS, using the correlation of a known sequence. The pseudorange ρ_l at the measurement instance t_k, is given by, [5]

$$\begin{aligned}\rho_l(t_k) &= \|\mathbf{r}_r(t_k) - \mathbf{r}_s^l(t_k - \tau_l(t_k))\| + c\left[\delta t_I^l(t_k) + \delta t_T^l(k)\right] \\ &+ c \cdot \left[\delta t_r(t_k) - \delta t_s^l(t_k - \tau_l(t_k))\right] + \nu_l(k), \\ &\quad l \in [1, L], k = 1, 2, ..., \end{aligned} \tag{1}$$

where $\nu_*(\cdot)$ represents the measurement noise, conveniently modeled as WGN with variance $\sigma_{\nu,l}^2$. Once the pseudorange from multiple satellites is obtained, one could use the classical multi-lateration technique [6] or other approximations like linearization [7] to estimate $\mathbf{r}_r(t_k)$.

2) Carrier Phase Measurement Model: Similar to Doppler, the carrier phase can be measured using data-driven and decision-directed methods [8], [9]. This carrier phase needs to be related to the position of the UT and the same can be obtained at the UT by using the time-of-flight. Using (1), the measured phase (scaled by c and having the units of distance) is related to pseudo-range through the modulo 2π operation prevalent in phase calculations. In this context, using (1), the *(scaled)* phase response takes the form,

$$\begin{aligned}\phi_l(k) &= \|\mathbf{r}_r(t_k) - \mathbf{r}_s^l(t_k - \tau_l(t_k))\| + c\left[\delta t_I^{l,i}(t_k) + \delta t_T^{l,i}(k)\right] \\ &+ c \cdot \left[\delta t_r^i(t_k) - \delta t_s^l(t_k - \tau_l(t_k))\right] + \lambda_l N_l \\ &+ \varrho_l(k), l \in [1, L], \forall k, \end{aligned} \tag{2}$$

with λ_l denoting the wavelength. It should be noted that the measurements suffer from integer ambiguity factor N_l and carrier-phase ambiguity mechanisms are needed. These mechanisms typically need additional resources; a classical approach is to consider double differences employing multiple satellites and receivers [1], [10].

3) Doppler Measurements: Classical algorithms exist for extracting Doppler frequency using the air-interface specifics, particularly the known symbol fields. Let $f_{D_l}(t)$ be the Doppler estimated for the l^{th} LEO satellite at time t. From the Doppler, pseudorange rate measurement $\dot{\rho}$ is obtained as [5],

$$\dot{\rho}_l(t) = -\frac{c}{f_c} f_{D_l}(t) \tag{3}$$

where f_c is the carrier frequency. Differentiating (1), an equivalent model for the pseudorange rate can be obtained as

$$\begin{aligned}\dot{\rho}_l(k) &= \frac{[\dot{\mathbf{r}}_r(t_k) - \dot{\mathbf{r}}_s^l(t_k - \tau_l(t_k))]^T [\mathbf{r}_r(t_k) - \mathbf{r}_s^l(t_k - \tau_l(t_k))]}{\|\mathbf{r}_r(t_k) - \mathbf{r}_s^l(t_k - \tau_l(t_k))]\|} \\ &+ c \cdot \left[\dot{\delta t}_r(t_k) - \dot{\delta t}_s^l(t_k - \dot{\tau}_l(t_k))\right] \\ &+ c \cdot \dot{\delta t}_I^l(t_k) + c \cdot \dot{\delta t}_T^l(k) + \varrho_l(k),\ l \in [1, L],\ \forall k, \end{aligned} \tag{4}$$

where the derivatives of variables w.r.t time t are denoted using a dot on the top and $\varrho_*(\cdot)$ is approximated as WGN with zero mean and variance $\sigma_{\varrho,l}^2$.

4) Sources of Error: Three types of errors arise in using LEO for PNT. These include

1) **Clock Bias and Drift:** Unlike GNSS, LEO system clocks are not tightly synchronized, particularly since it is not necessarily equipped with high-quality atomic clocks and uses commercial hardware at the receiver. Further, the clock errors (bias and drift) are unknown to the receiver, while information about parameters to be applied to satellite clock status for its correction and ionospheric models are embedded in GPS signals [11]. Typically the broadband system works in presence of these errors using synchronization loops often taking recourse to the air-interface structure.
2) **Ionospheric and Tropospheric Errors:** Most broadband LEO constellations reside above the ionosphere;this induces delays in their signals. Although LEO satellite signals propagate through the troposphere, its effect is less significant compared to ionospheric propagation. The magnitude of the ionospheric delay (i) varies as $\frac{1}{f_c^2}$ and (ii) is proportional to the rate of change of the obliquity factor. Since LEO constellations are planned in the Ku/ Ka/ V bands, compared to the L-band of GNSS, the ionospheric delays are lower. However, since the LEO satellites have larger velocities compared to GNSS, their obliquity factor changes faster than GNSS adding to the delay [1].

Any algorithm that aims to use LEO for PNT needs to include these sources of errors.

III. Pseudorange Rate based LEO PNT

Many of the aforementioned LEO PNT models have been investigated in literature; as mentioned earlier, these models are motivated by the GNSS methodologies. Typically, the carrier phase measurement is proposed to offer better accuracy than the pseudorange-based measurements when the ambiguities are resolved [12]. However, carrier phase-based recovery requires additional resources in terms of multi-band reception from the same source, multiple resources, etc. In the context of LEO PNT, the reception from each satellite is on a particular band and having multiple synchronized receivers is uncommon. In this context, the carrier phase-based methodologies may not be attractive from a system perspective.

From a signal processing perspective, it follows that the derivations in [13], that the Cramer-Rao Lower Bound (CRLB) for phase and frequency measurements, under ideal conditions, given respectively by σ_f^2 and σ_θ^2 below take the form,

$$\sigma_f^2 \propto \frac{1}{SNR} \times \frac{1}{N(N^2-1)} \quad (5)$$

$$\sigma_\theta^2 \propto \frac{1}{SNR} \times \frac{1}{N} \quad (6)$$

where N is the number of measurements and SNR denotes the signal-to-noise ratio at the processor input. In this context, for a given number of pilots in the air interface, (5), (6) indicate that the frequency measurement has much lower noise than phase measurement. In the current setting, the frequency estimate corresponds to the Doppler estimation, and hence pseudo-range rate offers a better measurement compared to the phase. Considering both the system level and signal processing aspects, the pseudorange rate-based approach is considered [1].

A. Extended Kalman Filter

Kalman filter and its extensions like the EKF, have been used extensively in radar tracking systems [14], [15]. The primary Kalman filter is the optimum choice if the states are linearly related to the measurements. However, considering (4), the measurement is highly non-linear in the potential state vector − location of the UT. Therefore, the basic Kalman filter is not suitable and the EKF is considered. In the EKF, the measurement function is approximated by its equivalent Jacobian matrix evaluated at the predicted state vector.

Following the literature, [14], [15], and building on the works [5], an Extended Kalman Filter (EKF) is used to obtain the estimates of the position using (4). As a first step, we consider the following simplification. As a first approximation, the variations in the ionospheric and tropospheric delays during LEO satellite visibility are negligible compared to the errors in the satellite's estimated velocities; hence, $\{\delta t_I, \delta t_T\}$ are ignored in the measurement. Further, the clock drifts of the stationary receiver and of the satellites are assumed to be constant. Furthermore, we assume the target to be stationary.

[1]The pseudorange based approach is not considered since timing information is assumed to be absent at the UT about the LEO transmission, unlike in GNSS

Under these assumptions, (4) takes the simplified form,

$$\dot{\rho}_l(k) = \frac{[\dot{\mathbf{r}}_s^l(t_k - \tau_l(t_k))]^T[\mathbf{r}_s^l(t_k - \tau_l(t_k)) - \mathbf{r}_r(t_k)]}{\|\mathbf{r}_r(t_k) - \mathbf{r}_s^l(t_k - \tau_l(t_k))]\|^2} + c \cdot \triangle\dot{\delta t}^l + \varrho_l(k), \quad l \in [1, L], k = 1, 2, ..., \quad (7)$$

where $\triangle\dot{\delta t}^l = \dot{\delta}_r - \dot{\delta}_s^l$ captures the effect of the clock drifts between the l^{th} satellite and the receiver. In GNSS, corrections to the orbital elements and clock errors are periodically transmitted to the receiver in a navigation message to determine the quantities $\mathbf{r}_s^l, \dot{\mathbf{r}}_s^l, \triangle\dot{\delta t}$. While the methodology to obtain $\mathbf{r}_s^l, \dot{\mathbf{r}}_s^l$ in LEO satellites systems bereft of the navigation message is presented in the sequel, the clock drift is compensated to a large extent by the synchronization loops and the resulting residual is modeled as an additional noise source. In view of this, the noise term $\varrho_l(k)$ in (7), will also include $c \cdot \triangle\dot{\delta t}^l$.

With these simplifications in mind, the following have been defined

1) **State vector**: In [5], the state vector at time instance t_k, defined as $\mathbf{x}(k)$, has the form $\mathbf{x}(k) = \mathbf{r}_r$. For the considered assumption, letting T be the sampling interval, the state evolution model is
$$\mathbf{x}(k+1) = \mathbf{x}(k). \quad (8)$$
2) **Measurements** at time instance t_k is denoted as $\mathbf{z}(k) = [\dot{\rho}_1(k), \dot{\rho}_2(k), \ldots, \dot{\rho_L}(k)]^T$. Let the measurement corresponding to the pseudorange rate of l^{th} satellite be abstracted as, $z_l(i) \triangleq \dot{\rho}_l(i) = f(\mathbf{x}(i)|\mathbf{r}_s^l(i), \dot{\mathbf{r}}_s^l(i)) + \varrho_l(i)$, where $f(\cdot)$ is a non-linear function of the state variables and parameterized by the satellite position and velocity. Toward obtaining a tractable solution, the non-linear function is replaced by its Jacobian, leading to a linearized measurement model in accordance with the principles of EKF modeling.

Subsequently, an EKF is designed to produce an estimate $\widehat{\mathbf{x}}(k|m), k > m$ of $\mathbf{x}(k)$ using all pseudorange rate measurements in $[1, m]$. This leads to the EKF updates, whose steps are presented in Algorithm 1 and follow the steps in [5]

It should be noted that, due to the state equation in (8), $\mathbf{Q}$ is ideally zero. However, in the simulations, $\mathbf{Q} = \sigma_q^2\mathbf{I}$ for some small σ_q^2 to enable tractable iterations [5].

1) Information needed for EKF: To exploit the aforementioned models on the use of LEO satellites for navigation, it follows from (1) - (4), that any planned algorithm would need one or more of the following:

1) $\widehat{\mathbf{r}}_s^l(\cdot)$: Position estimate of the LEO satellites
2) $\widehat{\dot{\mathbf{r}}}_s^l(\cdot)$: Velocities of the LEO satellites, $\dot{\mathbf{r}}_s^l(\cdot)$

The position of any satellite may be parameterized by its Keplerian elements [16]: semi-major axis, eccentricity, inclination, mean longitude, the longitude of perihelion, and the longitude of the ascending node. These elements are tracked, updated once daily, and made publicly available by the North American Aerospace Defense Command (NORAD) in the form of two-line element (TLE) files [17]. The information in these files is used to initialize a simplified general perturbation (SGP) model to propagate a satellite in its orbit. This model offers the estimates of position and velocity [1]. While the use of information from TLE and the use of SGP offers position and velocity estimates, errors do occur in their estimation.

Algorithm 1 EKF

Input: $\mathbf{x}(0), \mathbf{P}(0), \mathbf{Q}, \widehat{\mathbf{r}}_s^m(k), \widehat{\dot{\mathbf{r}}}_s^m(k), \forall m \in [1, L], \forall k$

repeat
  $\widehat{\mathbf{x}}(k|k-1) = \widehat{\mathbf{x}}(k-1|k-1)$ ▷ Predict State Estimate;
  $\mathbf{P}(k+1|k) = \mathbf{P}(k|k) + \mathbf{Q}$ ▷ Predict Covariance Estimate;
  $\widehat{\mathbf{z}}_k(k|k-1) \triangleq [\widehat{z}_k^1(k|k-1), \widehat{z}_k^2(k|k-1), \ldots, \widehat{z}_k^L(k|k-1)]$,
  $\widehat{z}_k^m(k|k-1) \triangleq f(\widehat{\mathbf{x}}(k|k-1)), \widehat{\mathbf{r}_s}^m(k), \widehat{\dot{\mathbf{r}}_s}^m(k)), m \in [1, L]$ ▷ Predicted Measurements ;
  $\mathbf{H}(k) = [\mathbf{h}_1(k), \mathbf{h}_2(k), \ldots, \mathbf{h}_L(k)], \mathbf{h}_m(k) = \frac{\partial f(\mathbf{x}, \mathbf{r}_s^l)}{\partial x}|_{[\mathbf{x}=\widehat{\mathbf{x}}(k|k-1), \mathbf{r}_s^m(k)=\widehat{\mathbf{r}}_s^m(k), \dot{\mathbf{r}}_s^m(k)=\widehat{\dot{\mathbf{r}}}_s^m(k)]}$ ▷ Jacobian;
  $\boldsymbol{\xi}(k) \triangleq \mathbf{z}(k) - \widehat{\mathbf{z}}_k(k|k-1)$ ▷ Innovation Term;
  $\mathbf{S}(k) = \mathbf{H}(k)\mathbf{P}(k|k-1)\mathbf{H}^T(k) + \mathbf{R}(k)$ ▷ Residual Covariance;
  $\mathbf{K}(k) = \mathbf{P}(k|k-1)\mathbf{H}^T(k)[\mathbf{S}(k)]^{-1}$ ▷ EKF gain;
  $\widehat{\mathbf{x}}(k|k) = \widehat{\mathbf{x}}(k|k-1) + \mathbf{K}(k)\boldsymbol{\xi}(k)$ ▷ Updated State Estimate ;
  $\mathbf{P}(k|k) = (\mathbf{I} - \mathbf{K}(k)\mathbf{H}(k))\mathbf{P}(k|k-1)$ ▷ Updated Covariance;
until

This is predominantly due to the use of simplified models of perturbing forces; these cause errors in a propagated satellite orbit as high as three kilometers.

B. Impact on Air Interface

In the following, we briefly consider the impact of pseudorange rate-based measurements on the air interface. Doppler estimation in this context differs from those in classical radar in the sense of received Signal-to-Noise-Ratio (SNR). In the communication context, the SNR is sort of guaranteed by the link budget, while in a classical radar context, the non-coherent scattering involves a fourth-order decay of power with distance typically leading to negative SNR at the front end. In this context, the current application is well placed, and the need for pulse compression to build SNR, as in the radar context, is not mandatory, but a good-to-have feature.

The Doppler of LEO satellites is in of the range $[-300, 300]$ kHz and the Doppler rate is about 3.5 kHz/s. Assuming a variation of f_{tol} Hz in Doppler as being acceptable within a frame to consider a line spectrum estimation, it follows that the frame rate F (in frame/sec) needed is $F \geq \frac{3500}{f_{tol}}$ under the assumption of one Doppler estimate per frame. Further, the estimation error varies as N^{-3}, where N is the number of symbols used for estimation. In most of the satellite standards, blocks of pilots are distributed over the entire frame and not as singletons. Considering the current DVB-S2x Superframe Format comprising a total of 612540 symbols bundled into a number of frames (9 for format 2, 36 for format 3) [18], the Doppler can be estimated on

- Start of Super Frame typically has 270 known symbols
- Uncoded pilots interspersed within each bundled frame whose number is dependent on the superframe format. Format 2 has 71 fields, each of 36 symbols separated by 920 symbols while format 3 has 9 fields, each of 48 symbols separated by 1839 symbols [18].

Thus each bundled frame has sufficient pilots to estimate Doppler. Further, assuming $f_{tol} \approx 3.5$ Hz, the number of bundled frames (each offering a Doppler estimate) needs to be approximately 1000/s, which, would lead to about 64 MSps for the largest bundled frame format 2 and 16 MSps for the format 3. The proprietary air-interface-based Starlink is claimed to offer between 40-90 MSps [19]. Finally, the measurement for Doppler should be sampled sufficiently to avoid aliasing. Considering these aspects, it can be deduced that a single Doppler frequency can be estimated over a single bundled frame.

IV. Simulation Results

In the representative results provided below, we consider a simple set-up where the user terminal to be localized is at $\mathbf{s} = [1, -2, 3]^T$. We consider N satellites, henceforth referred to as objects, with ith object having its initial location at $\mathbf{r}_s^i(0)$, the initial velocity vector (Cartesian coordinate system) being $\dot{\mathbf{r}}_s^i(0)$ and acceleration vector being $\mathbf{a}_i$. These entries are chosen randomly as $\mathbf{r}_s^i(0) \sim \mathcal{U}(-1000, 1000), \dot{\mathbf{r}}_s^i(0) \sim \mathcal{U}(-70, 70)$ and $\mathbf{a}_i \sim \mathcal{U}(-70, 70)$, where $\mathcal{U}(a, b)$ denotes an uniform distribution in the range $[a, b]$. The measurement error variance is given by $\sigma_r^2 \triangleq \sigma_{\varrho,l}^2, \forall l$, and the process noise variance is σ_q^2. In the following, we evaluate the impact of different N, σ_q and σ_r on localization accuracy.

A. Dependence on the number of satellites

It is evident that the larger the number of independent variables, better is the localization accuracy. This can be seen in Fig. 1 - 3 where the localization accuracy improves as N goes from 4 to 12; further, $\sigma_q = 0.1$ and $\sigma_r = 0.1$ in these plots. An extensive simulation on these lines can enable a system designer to choose the minimum number of satellites needed to achieve this additional objective of lower efficiency.

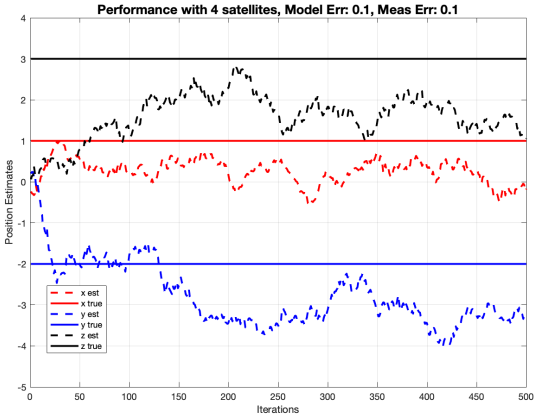

Fig. 1. Localization MSE in the three coordinates for $N = 4$ satellites

B. Dependence on the Model/ Processing error

We now consider the impact of model/ processing error in Fig. 3-4, for $N = 12$ satellites and $\sigma_r = 0.1$; herein, we consider two different values of σ_q. As can be seen in these figures, the performance is rather susceptible to model errors.

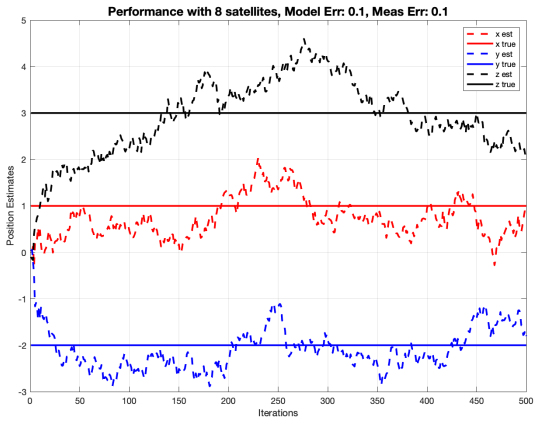

Fig. 2. Localization MSE in the three coordinates for $N = 8$ satellites

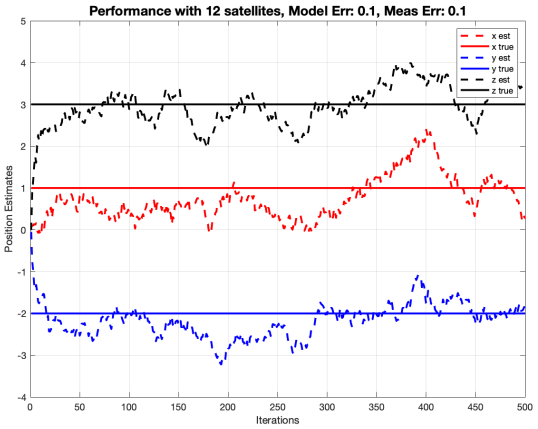

Fig. 3. Localization MSE in the three coordinates for $N = 12$ satellites

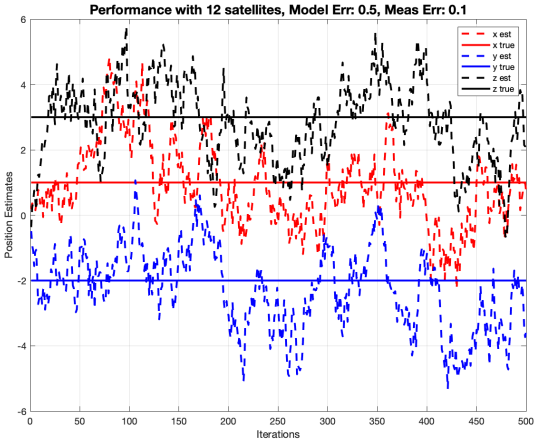

Fig. 4. Localization MSE in the three coordinates for $N = 12$ satellites

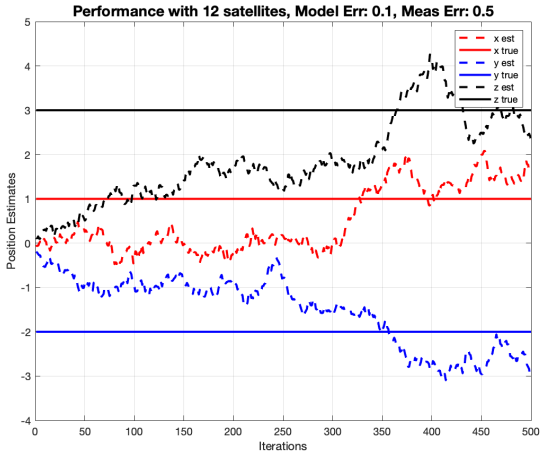

Fig. 5. Localization MSE in the three coordinates for $N = 12$ satellites

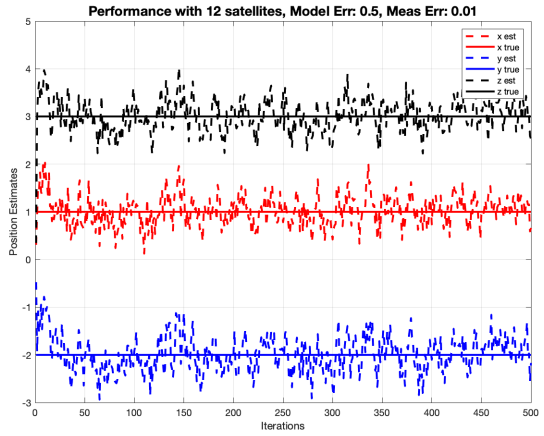

Fig. 6. Localization MSE in the three coordinates for $N = 12$ satellites

C. Dependence on the Measurement error

We now consider the impact of measurement error in Fig. 3 and 5, for $N = 12$ measurements and $\sigma_q = 0.1$; herein, we consider two different values of σ_r. The performance degradation due to increased measurement error is highlighted.

Finally, Fig. 6 depicts the performance of the localization for $\sigma_q = 0.5$ and $\sigma_r = 0.01$. It can be seen that the localization error is rather small compared to the case of $\sigma_q = 0.1, \sigma_r = 0.1$ in Fig. 3 and $\sigma_q = 0.5, \sigma_r = 0.1$ in Fig. 4. This indicates, under the current set-up, the system is more prone to measurement errors than modeling errors.

V. Conclusions

This study approached the idea of LEO PNT from two fronts: (a) an academic perspective and (b) a system perspective. Based on the notions from GNSS, the different PNT models are presented, and using the broadband satellite receiver operations, the system model is developed and the system impact of undertaking the opportunistic PNT is assessed. Following a signal processing perspective, a particular model based on pseudorange rate is pursued and initial EKF-based implementation showed promise for the LEO localization. Future work would be to further elaborate the tracking and

relate air-interface performance on Doppler estimation (CRLB/ RMSE) into the localization algorithm.

REFERENCES

[1] Z. Kassas, J. Morales, and J. Khalife, "New-age satellite-based navigation–stan: simultaneous tracking and navigation with leo satellite signals," *Inside GNSS Magazine*, vol. 14, no. 4, pp. 56–65, 2019.

[2] B. Hofmann-Wellenhof, H. Lichtenegger, and E. Wasle, *GNSS – Global Navigation Satellite Systems*. Springer Verlag, Austria, 2008.

[3] Z. Kassas, J. Khalife, M. Neinavaie, and T. Mortlock, "Opportunity comes knocking: overcoming GPS vulnerabilities with other satellites' signals," *Inside Unmanned Systems Magazine*, pp. 30–35, July 2020.

[4] Z. Kassas, M. Neinavaie, J. Khalife, N. Khairallah, S. Kozhaya, J. Haidar-Ahmad, and Z. Shadram, "Enter leo on the gnss stage: navigation with starlink satellites," *Inside GNSS Magazine*, pp. 42–51, Dec 2021.

[5] J. J. Khalife and Z. M. Kassas, "Receiver design for doppler positioning with leo satellites," in *ICASSP 2019 - 2019 IEEE International Conference on Acoustics, Speech and Signal Processing (ICASSP)*, 2019, pp. 5506–5510.

[6] S. Bancroft, "An algebraic solution of the gps equations," *IEEE Transactions on Aerospace and Electronic Systems*, vol. AES-21, no. 1, pp. 56–59, 1985.

[7] A. M. El-naggar, "An alternative methodology for the mathematical treatment of gps positioning," *Alexandria Engineering Journal*, vol. 50, no. 4, pp. 359–366, 2011. [Online]. Available: https://www.sciencedirect.com/science/article/pii/S1110016811000470

[8] U. Mengali and A. N. D' Andrea, *Synchronization Techniques for Digital Receivers*. Springer New York, NY, 1997.

[9] E. Casini, R. D. Gaudenzi, and A. Ginesi, "Dvb-s2 modem algorithms design and performance over typical satellite channels," *International Journal of Satellite Communications and Networking*, vol. 22, no. 3, pp. 281–318, 2004. [Online]. Available: https://onlinelibrary.wiley.com/doi/abs/10.1002/sat.791

[10] P. Teunissen, "Theory of carrier phase ambiguity resolution," *Wuhan University Journal of Natural Sciences*, vol. 8, pp. 471–484, 06 2003.

[11] GPS Navigation Message. [Online]. Available: https://gssc.esa.int/navipedia/index.php/GPS_Navigation_Message

[12] G. Blewitt, "Carrier phase ambiguity resolution for the global positioning system applied to geodetic baselines up to 2000 km," *Journal of Geophysical Research: Solid Earth*, vol. 94, no. B8, pp. 10 187–10 203, 1989.

[13] F. Rice, B. Cowley, B. Moran, and M. Rice, "Cramer-rao lower bounds for QAM phase and frequency estimation," *IEEE Transactions on Communications*, vol. 49, no. 9, pp. 1582–1591, 2001.

[14] S. J. Julier and J. K. Uhlmann, "New extension of the Kalman filter to nonlinear systems," in *Signal Proces., sensor fusion, target recognition*, vol. 3068. Int. Soc. Optics Photon., 1997, pp. 182–194.

[15] M. A. Richards, *Fundamentals of radar signal processing*. Tata McGraw-Hill Education, 2005.

[16] Approximate positions of the planets. [Online]. Available: https://ssd.jpl.nasa.gov/planets/approx_pos.html

[17] Description of the NORAD two-line element format. [Online]. Available: http://celestrak.org/NORAD/documentation/

[18] "ETSI en 302307-2, digital video broadcasting (dvb); "second generation framing structure, channel coding and modulation systems for broadcasting, interactive services, news gathering and other broadband satellite applications; part II: S2-extensions (S2-X)," ETSI, Tech. Rep., 2014.

[19] R. Kraus. New speedtest data show starlink internet speeds and latency are all over the place. [Online]. Available: https://mashable.com/article/starlink-internet-latency-speedtest